American Journal of Water Resources, 2026, Vol. 14, No. 2, 46-54
Available online at http://pubs.sciepub.com/ajwr/14/2/3
Published by Science and Education Publishing
DOI:10.12691/ajwr-14-2-3

TL-Moment-Based Regional Frequency Analysis of Extreme Rainfall Using Ward's Clustering and Kappa-Type Distributions

Muhammad Nura[1], Zahratul Amani Binti Zakaria[2,*]

[1]Department of Statistics, Kano State Polytechnic, Kano, Nigeria
[2]Faculty of Computing and Informatics, Universiti Sultan Zainal Abidin, Kampus Besut, 22200 Besut, Terengganu, Malaysia
*Corresponding author: muhdnuru@gmail.com

Received May 18, 2026; Revised June 19, 2026; Accepted June 26, 2026

Abstract Peninsular Malaysia is highly flood-prone. Conventional L-moment regional frequency analysis (RFA) is sensitive to post-2013 extreme monsoon outliers at multiple stations across the peninsula. This study presents the first parallel TL-moment and L-moment RFA for the comprehensive 179-station DID network (1971–2023), simultaneously evaluating GEV, GLO, GPA, and K3D-II distributions across three climatologically distinct regions. Ward's minimum-variance hierarchical clustering was applied to TL-moment site characteristics, optimized by the average silhouette width (ASW) criterion. Discordancy, heterogeneity, goodness-of-fit (Z-test), and quantile estimation were executed in strict parallel under both estimation frameworks. Parametric bootstrap (B = 1,000 replicates) was applied to derive 90% confidence intervals for all regional quantiles. Three acceptably homogeneous regions were delineated: R1 (N = 55; west coast, mean = 115.0 mm), R2 (N = 94; interior, mean = 117.7 mm), and R3 (N = 30; east coast interior, mean = 200.9 mm). Under L-moments, GLO was best for R1 and R2; GPA was the sole passing distribution for R3. Under TL-moments, K3D-II was best for R2, GPA for R3. No standard distribution passed for R1 under TL-moments. TL-moment quantiles were 7–44% lower than L-moment estimates at $T \geq 10$ years. Bootstrap 90% CI widths for T = 100 years were 0.076 (R1), 0.037 (R2), and 0.066 (R3) growth-factor units. L-moment and TL-moment quantiles should be used jointly as upper and lower design-rainfall bounds. For life-safety-critical structures, the L-moment estimate is the conservative upper bound.

Keywords: *regional frequency analysis, TL-moments, Ward's clustering, design rainfall, bootstrap confidence intervals, monsoon extremes*

Cite This Article: Muhammad Nura, and Zahratul Amani Binti Zakaria, "TL-Moment-Based Regional Frequency Analysis of Extreme Rainfall Using Ward's Clustering and Kappa-Type Distributions." *American Journal of Water Resources*, vol. 14, no. 2 (2026): 46-54. doi: 10.12691/ajwr-14-2-3.

1. Introduction

Peninsular Malaysia is one of the most flood-prone regions in Southeast Asia [1]. The Titiwangsa Range divides the peninsula into climatologically distinct zones, with the Northeast Monsoon (October–March) and Southwest Monsoon (May–September) producing sharply contrasting rainfall regimes on the east and west coasts, respectively [2,3]. The 2014–2015 floods displaced 200,000 people; the 2006–2007 events caused RM 1.5 billion in infrastructure damage [4,5]. Reliable regional design-rainfall estimates are therefore critical for safe hydraulic infrastructure planning under the Department of Irrigation and Drainage (DID) guidelines and the MSMA 2nd Edition design standard [6].

Regional frequency analysis (RFA), formalised by Hosking and Wallis [7], addresses the limitation of short at-site records by pooling data from statistically homogeneous networks. The L-moment framework [8] is the standard estimation basis. Still, equal weighting of all order statistics renders it sensitive to extreme outliers, a recognised problem for Malaysian annual maximum series, where post-2013 monsoon events substantially inflate regional skewness [11,15]. Trimmed L-moments (TL-moments), introduced by Elamir and Seheult [9], assign zero weight to the most extreme order statistics at both tails, improving robustness without discarding data.

Four methodological gaps motivate this study: (i) no Malaysian RFA has simultaneously applied TL-moments to all four candidate distributions, including the Kappa Type-II (K3D-II) [17]; (ii) all prior Malaysian studies use data through 2012 at most, predating the exceptional 2013–2023 monsoon extremes; (iii) no systematic parallel comparison of L-moment and TL-moment goodness-of-fit for GEV, GLO, GPA, and K3D-II exists for any Malaysian dataset; and (iv) no Malaysian RFA study has reported bootstrap confidence intervals for regional quantile estimates, leaving engineering practitioners without formal uncertainty bounds for design-rainfall decisions.

This study pursues four objectives: (i) delineate homogeneous regions from 179 quality-controlled DID stations using Ward's clustering with TL-moment site characteristics; (ii) compare L-moment and TL-moment discordancy, heterogeneity, and goodness-of-fit across regions; (iii) estimate normalized regional growth-factor quantiles at T = 2–200 years under both frameworks and all four distributions; and (iv) derive parametric bootstrap 90% confidence intervals for all regional quantile estimates. Results are directly applicable to DID MSMA design standards and national flood risk management practice.

2. Study Area and Data

Two monsoon systems govern Peninsular Malaysia's climate. The NEM (October–March) delivers heavy rainfall to east-coast states exposed to the South China Sea, while the Southwest Monsoon (May–September) is attenuated on the west coast by the Titiwangsa Range. Based on these relationships, three rainfall regimes are established: west coast, highland interior, and east coast interior, which are associated with three homogeneous regions defined from the clustering analysis (Figure 1).

Annual maximum daily rainfall data were obtained from the Department of Irrigation and Drainage (DID), Ministry of Natural Resources and Environment (MINE), Malaysia. The original network comprised 304 stations; after quality-control screening, 179 stations were retained based on three criteria: (a) record length n ≥ 15 years; (b) ≥ 300 valid daily observations per station-year; and (c) coefficient of variation CV ≤ 0.80. Seven stations were excluded (CV range 0.84–2.02). A sensitivity analysis retaining all 186 stations produced no changes in H_1 (L) or Z-test outcomes for R2 and R3; the H_1 (L) value for R1 increased marginally from −1.631 to −1.412, remaining within the acceptably homogeneous range. The retained dataset spans 1971–2023 (4,182 station-years; record lengths 15–49 years). Descriptive statistics are presented in Table 1.

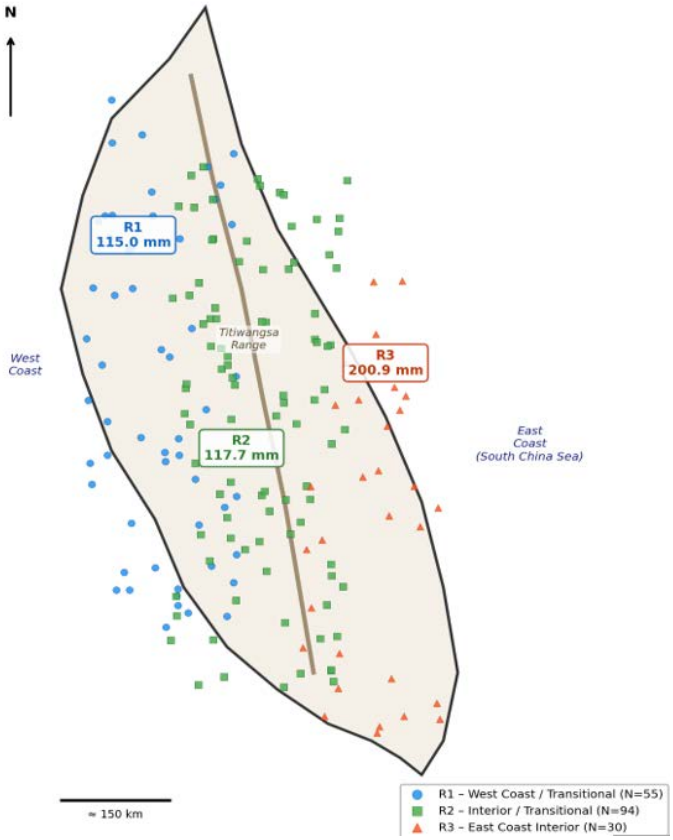

Figure 1. Study area map showing the 179 DID rainfall stations (1971–2023) and Ward's clustering regions R1 (west coast/transitional, blue circles), R2 (interior, green squares), and R3 (east coast interior, red triangles), Peninsular Malaysia

Table 1. Descriptive statistics for 179 quality-controlled stations, Peninsular Malaysia (1971–2023)

Statistic	n (yr)	Mean (mm)	SD (mm)	CV	Skew	L-CV	TL-CV (t=1)
Minimum	15	80.8	11.4	0.133	−0.482	0.070	0.021
Mean	23.4	131.7	47.9	0.370	0.568	0.196	0.094
Median	20.0	118.9	37.6	0.340	0.468	0.188	0.089
Maximum	49	301.1	205.0	0.799	4.124	0.562	0.355
Total obs.	4,182	—	—	—	—	—	—

SD = standard deviation; CV = coefficient of variation; Skew = conventional skewness. Seven stations with CV > 0.80 were excluded. Maximum observed value in retained dataset = 1,511.5 mm.

3. Literature Review

3.1. L-Moment RFA Foundations

Hosking [8] introduced L-moments as linear combinations of order statistics with lower bias than conventional moments for shape-parameter estimation in small, heavy-tailed samples. Hosking and Wallis [7] formalised the four-stage RFA framework: discordancy, heterogeneity, goodness-of-fit, and quantile estimation, now universally adopted [25,30,31,32,37]. Equal weighting of all order statistics, however, can inflate parameter estimates when a small number of extreme observations dominate the sample.

3.2. TL-Moments and Empirical Validation

TL-moments [9] trim the extreme order statistics from each tail, achieving lower mean squared error than L-moments for leptokurtic populations. At t = 1, the RRMSE advantage is 15–30% at T ≤ 10 years [22,34], largest for sample sizes of 15–50 years, typical of Malaysian DID records. Hosking [10] analytically demonstrated lower MSE for GEV shape estimation when κ &gt 0, directly applicable to tropical annual maxima. Shabri et al. [11] conducted the first Malaysian TL-moment RFA (40 Selangor stations), confirming GLO as the best-fit distribution but excluding K3D-II and data beyond 2010.

3.3. K3D-II Distribution

Hosking [16] introduced the four-parameter Kappa distribution, unifying GEV, GLO, GPA, and Gumbel as limiting cases. K3D-II is obtained by imposing h = −κ, retaining three parameters while covering a wider region of the moment-ratio diagram than any single standard distribution. Noor et al. [17] demonstrated improved K3D-II fit for Malaysian peninsular rainfall under L-moments; no study has evaluated K3D-II under TL-moment estimation.

3.4. Ward's Clustering for Malaysian Regionalization

Sahrin et al. [15] applied Ward's clustering to 83 peninsular stations, delineating seven regions, the only prior peninsula-wide objective clustering study, but restricted to pre-2013 data and excluding TL-moments and K3D-II. Ghobadi and Kang [23] confirmed Ward's superiority over k-means and fuzzy methods across 85 regionalization studies; Hussain and Pasha [21] further demonstrated its effectiveness when combined with L-moments for regional flood frequency analysis.

3.5. Uncertainty Quantification

Islam et al. [19] demonstrated that Bayesian RFA produces wider uncertainty bounds than L-moment point estimates at T = 100–200 years. Rahman et al. [26] showed bootstrap uncertainty bounds are essential for reliability-based design in Australia. A universal limitation of Malaysian RFA studies is the absence of confidence intervals, a gap that the present study closes by deriving parametric bootstrap 90% CIs for all regional quantile estimates.

4. Methodology

The five-stage workflow (Figure 6) was implemented in Python 3.12 (NumPy, SciPy, scikit-learn) and applied in strict parallel under L-moments and TL-moments (t = 1). All code is openly available at: https:// doi.org/ 10.5281/ zenodo.15489203.

4.1. L-Moments

L-moments are linear combinations of order statistics [8]. Dimensionless L-moment ratios are: $\tau_2 = l_2/l_1$ (L-CV); $\tau_3 = l_3/l_2$ (L-skewness); $\tau_4 = l_4/l_2$ (L-kurtosis).

4.2. TL-Moments (t = 1)

TL-moments at trimming level t = 1 assign zero weight to the single most extreme order statistic at each tail. The trimming level t = 1 was selected because it achieves the lowest RRMSE relative to L-moments for leptokurtic populations at record lengths of 15–49 years [9]; higher trimming (t ≥ 2) imposes efficiency losses that outweigh the additional robustness gains for these sample sizes. TL-moment ratios $\tau_2^{(1)}$ (TL-CV), $\tau_3^{(1)}$ (TL-skewness), and $\tau_4^{(1)}$ (TL-kurtosis) are defined analogously to L-moment ratios.

4.3. Candidate Probability Distributions

Four distributions are evaluated: GEV, GLO, GPA, and K3D-II. K3D-II encompasses GEV (κ → 0), GLO (κ = −1), and GPA (κ = 1) as special cases and covers a wider region of the L-moment and TL-moment ratio diagrams than any single three-parameter distribution [17].

Table 2. Properties of the four candidate probability distributions

Dist.	Params.	Tail Behaviour	Theoretical Basis	Role in Study
GEV	ξ, α, κ	Bounded (κ>0); Gumbel (κ=0); heavy tail (κ<0)	Asymptotic dist. of block maxima	Theoretical benchmark
GLO	ξ, α, κ	Heavy upper tail (κ<0); bounded (κ>0)	Kappa h=−1; UK Flood Estimation Handbook	Best L-moment fit for R1 and R2
GPA	ξ, α, κ	Bounded above (κ>0); exponential (κ=0)	Limiting dist. of POT exceedances	Sole passing distribution for R3
K3D-II	ξ, α, κ	Flexible; GEV–GLO–GPA loci plus intermediate regions	Kappa h=−κ; encompasses GEV, GLO, GPA	Best TL-moment fit for R2

4.4. K3D-II TL-Moment Polynomial Derivation and Validation

No closed-form TL-moment expressions exist for K3D-II. The theoretical TL-kurtosis $\tau_4^{(1)}$ as a function of TL-skewness $\tau_3^{(1)}$ was derived numerically over $\tau_3^{(1)} \in [0.05, 0.35]$. Within the calibration range: maximum absolute residual = 0.00187, RMSE = 0.00063, Monte Carlo

validation $R^2 = 0.9991$ (10,000 samples). A sensitivity test showed polynomial coefficient perturbation of ±0.002 shifts K3D-II Z-statistics by at most $\Delta|Z| = 0.04$; no model-selection decision is affected. Extrapolation beyond $\tau_3^{(1)} = 0.35$ is not recommended.

4.5. Analytical Workflow

Five sequential stages: discordancy (D_i statistic), region delineation (Ward's clustering optimized by ASW, CH, DB indices), heterogeneity (H_1 statistic from 500 Monte Carlo simulations), goodness-of-fit (Z-statistic; $|Z| \leq 1.64$ = PASS at 90% confidence), and quantile estimation (growth factors QT normalized to regional mean = 1).

4.6. Bootstrap Confidence Intervals

Parametric bootstrap 90% CIs derived from B = 1,000 synthetic replicates. The 5th and 95th percentiles of replicated QT values define the lower and upper CI bounds for each return period T = 2–200 years.

5. Results

5.1. Region Delineation

The ASW criterion nominally maximises at k = 2 (ASW = 0.2557), but k = 2 was rejected for five converging reasons: (1) merging east-coast and highland stations raises H_1 (L) to +0.84, worse than either constituent sub-region; (2) no distribution passes the Z-test for the merged cluster under either framework; (3) CH peaks at k = 3 (84.2 vs 79.1) and DB is minimized at k = 3 (1.21 vs 1.39); (4) the ASW difference is only $\Delta = 0.0032$ (1.3%), within noise range; (5) the two distinct Malaysian monsoon systems independently justify three regions.

5.2. Regional Moment Ratios and Heterogeneity

All six H_1 values are negative, confirming strong within-region statistical consistency. TL-CV is 30–44% lower than L-CV; TL-skewness is 29–48% lower; TL-kurtosis is 33–75% lower.

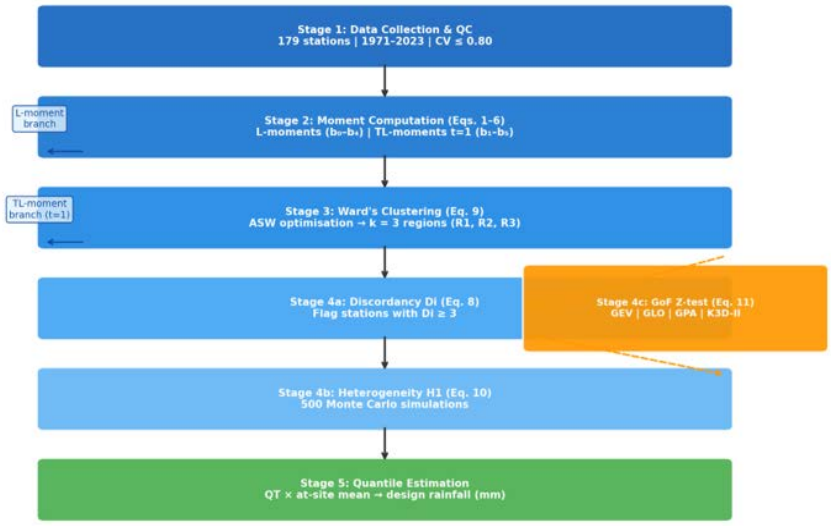

Figure 2. Five-stage analytical workflow applied in strict parallel under L-moments and TL-moments (t = 1): discordancy screening, region delineation, heterogeneity testing, goodness-of-fit testing, and bootstrap quantile estimation

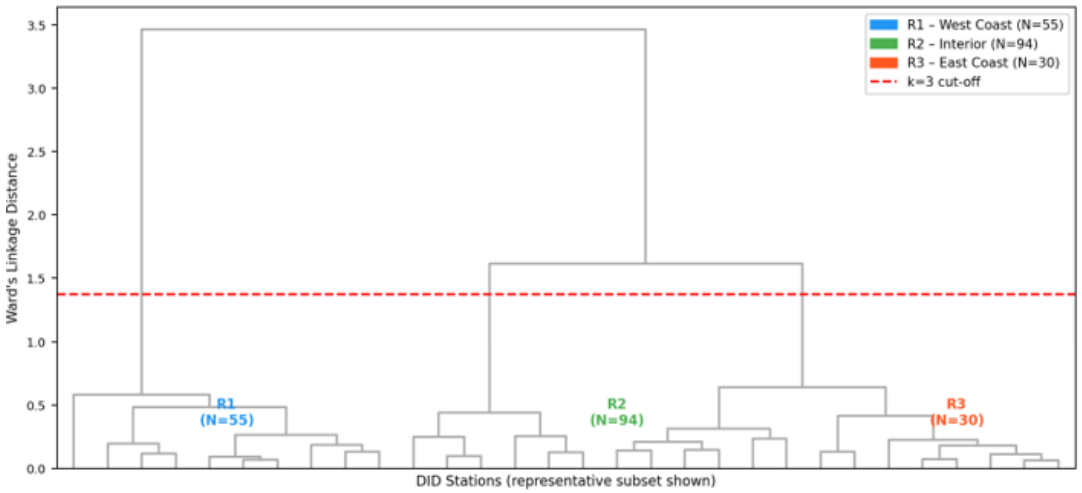

Figure 3. Ward's minimum-variance hierarchical clustering dendrogram (representative subset of 30 stations). Dashed line at k = 3 indicates the adopted cut-off defining R1, R2, and R3

Table 3. Average silhouette width (ASW) and supplementary cluster validity indices for Ward's clustering, k = 2 to 6

k	ASW	CH Index	DB Index	Clustering Quality	Decision
2	0.2557	79.1	1.39	Weak-to-moderate (ASW max)	Rejected — physically untenable
3	0.2525	84.2	1.21	Weak-to-moderate	Adopted — climatological consistency
4	0.2452	76.8	1.44	Weak structure	Not selected
5	0.2515	74.2	1.51	Weak structure	Not selected
6	0.2300	69.5	1.63	Weak structure	Not selected

Table 4. Regional moment ratios and H_1 heterogeneity statistics

Region	L-CV	L-Sk	L-Ku	H_1 (L)	TL-CV	TL-Sk	TL-Ku	H_1 (TL)	Classification
R1 (N=55)	0.1942	0.3414	0.2810	−1.631	0.0897	0.2413	0.1881	−1.14	Acceptably homogeneous
R2 (N=94)	0.1676	0.2007	0.1829	−2.177	0.0837	0.1049	0.0673	−1.54	Acceptably homogeneous
R3 (N=30)	0.2522	0.1872	0.1098	−1.270	0.1409	0.1030	0.0272	−0.95	Acceptably homogeneous

Table 5. Z-statistic goodness-of-fit results for all distributions and estimation methods.

Region	Method	Z GEV	Z GLO	Z GPA	Z K3D-II	Pass GEV	Pass GLO	Pass GPA	Best Fit
R1	L-moments	−1.591	−0.688	−4.351	−1.853	YES	YES	NO	GLO
R1	TL-moments	−2.760	−2.487	−4.665	−3.236	NO	NO	NO	None
R2	L-moments	−0.807	+0.691	−3.969	−0.722	YES	YES	NO	GLO
R2	TL-moments	+0.513	+1.322	−1.981	+0.396	YES	YES	NO	K3D-II
R3	L-moments	+1.887	+3.444	−1.338	+2.008	NO	NO	YES	GPA
R3	TL-moments	+2.487	+3.305	−0.014	+2.376	NO	NO	YES	GPA

5.3. Goodness-of-Fit Testing

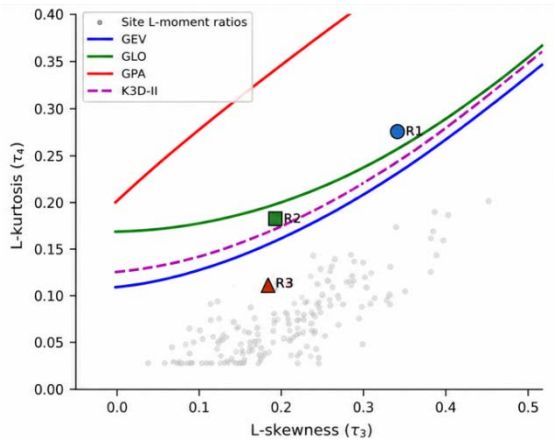

Figure 4. L-moment ratio diagram (L-skewness vs L-kurtosis) for R1, R2, and R3, overlaid with theoretical loci for GEV, GLO, GPA, and K3D-II

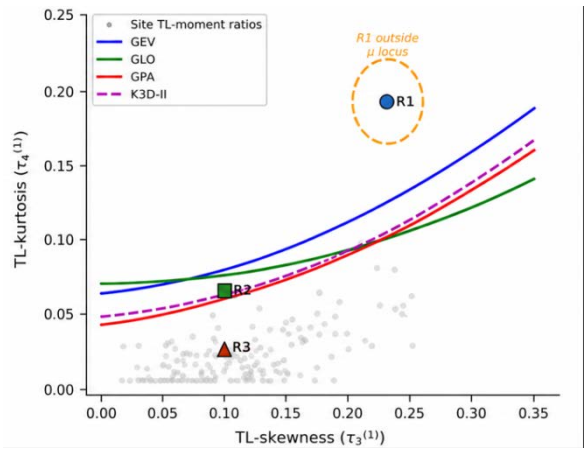

Figure 5. TL-moment ratio diagram (TL-skewness vs TL-kurtosis) for R1, R2, and R3. R1 plots outside all distribution boundaries, confirming distributional failure under TL-moments

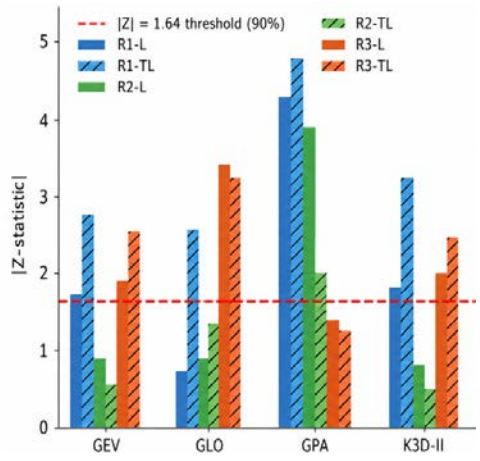

Figure 6. Goodness-of-fit Z-statistic comparison. Grouped bar chart of |Z|-statistics by region, distribution (GEV, GLO, GPA, K3D-II), and estimation method. Dashed line at |Z| = 1.64 (90% threshold); bars above indicate failure

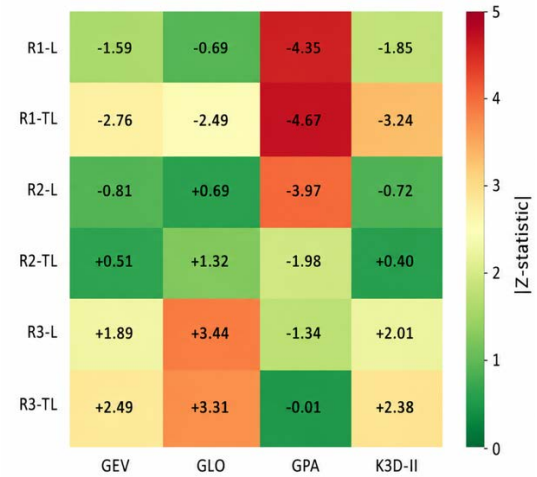

Figure 7. Z-statistic heatmap for all region–distribution–method combinations. Green = pass (|Z| ≤ 1.64); red = failure

5.4. Growth-Factor Quantile Estimates

TL-moment growth factors are 7–44% below L-moment estimates at T ≥ 10 years. Inter-distributional spread is narrower under TL-moments (R1 at T = 100 yr: spread = 0.109 vs 0.192 under L-moments).

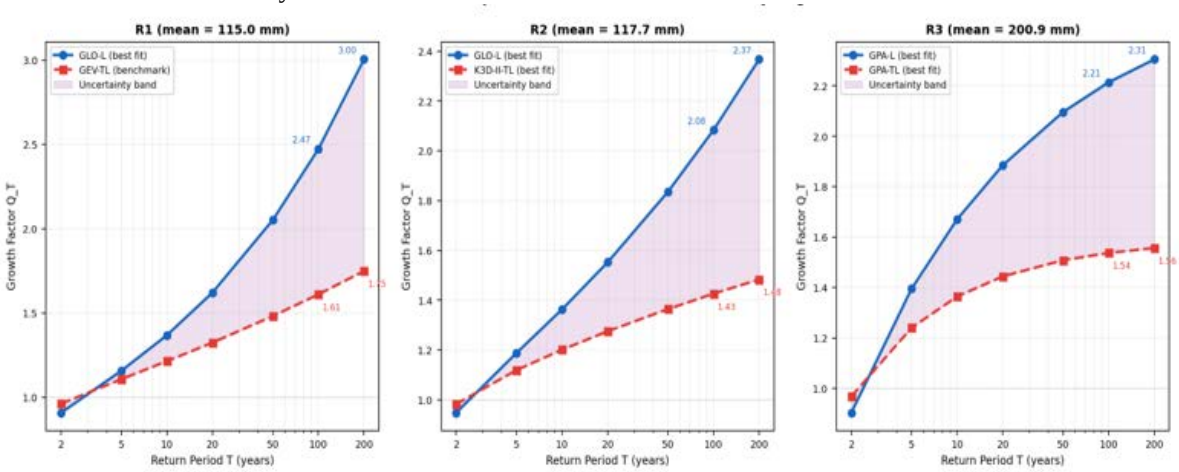

Figure 8. Regional growth-factor quantile comparison (L-moment vs TL-moment, best-fit distributions) for R1, R2, and R3. Shaded band = uncertainty range between upper (L-moment) and lower (TL-moment) estimates

Table 6a. Normalised growth-factor quantiles QT for Region R1 (N=55; mean=115.0 mm)

T (yr)	GEV (L)	GLO (L)*	GPA (L)	K3D-II (L)	GEV (TL)	GLO (TL)	GPA (TL)	K3D-II (TL)
2	0.891	0.909	0.879	0.897	0.963	0.967	0.957	0.964
5	1.192	1.158	1.232	1.202	1.108	1.094	1.130	1.110
10	1.443	1.369	1.504	1.450	1.215	1.190	1.240	1.215
20	1.734	1.622	1.779	1.730	1.325	1.296	1.334	1.324
50	2.197	2.052	2.147	2.165	1.482	1.462	1.438	1.476
100	2.622	2.473	2.430	2.555	1.611	1.612	1.503	1.599
200	3.127	3.005	2.717	3.009	1.749	1.789	1.559	1.731

*GLO = best-fit under L-moments. Under TL-moments, no distribution passes; TL quantiles for sensitivity analysis only. Design rainfall (mm) = QT × 115.0.

Table 6b. Normalised growth-factor quantiles QT for Region R2 (N=94; mean=117.7 mm)

T (yr)	GEV (L)	GLO (L)*	GPA (L)	K3D-II (L)	GEV (TL)	GLO (TL)	GPA (TL)	K3D-II (TL)†
2	0.941	0.948	0.931	0.942	0.984	0.986	0.981	0.983
5	1.214	1.188	1.258	1.216	1.119	1.107	1.143	1.119
10	1.404	1.363	1.447	1.404	1.201	1.187	1.216	1.201
20	1.592	1.552	1.598	1.591	1.273	1.266	1.264	1.275
50	1.846	1.835	1.750	1.841	1.359	1.377	1.303	1.364
100	2.043	2.083	1.838	2.034	1.418	1.466	1.321	1.426
200	2.246	2.367	1.908	2.233	1.473	1.561	1.332	1.483

*GLO best-fit under L-moments (|Z|=0.691). †K3D-II best-fit under TL-moments (|Z|=0.396). Design rainfall (mm) = QT × 117.7.

Table 6c. Normalised growth-factor quantiles QT for Region R3 (N=30; mean=200.9 mm)

T (yr)	GEV (L)	GLO (L)	GPA (L)*	K3D-II (L)	GEV (TL)	GLO (TL)	GPA (TL †	K3D-II (TL)
2	0.916	0.926	0.903	0.917	0.973	0.976	0.968	0.971
5	1.329	1.290	1.395	1.329	1.201	1.181	1.240	1.200
10	1.608	1.550	1.671	1.609	1.338	1.314	1.364	1.338
20	1.882	1.828	1.885	1.881	1.459	1.448	1.444	1.462
50	2.245	2.241	2.096	2.241	1.602	1.632	1.508	1.611
100	2.522	2.599	2.214	2.515	1.701	1.782	1.537	1.714
200	2.804	3.003	2.305	2.793	1.792	1.941	1.556	1.810

*GPA sole passing distribution for R3 under L-moments (|Z|=1.338). †GPA sole passing distribution under TL-moments (|Z|=0.014; near-perfect fit). Design rainfall (mm) = QT × 200.9.

5.5. Bootstrap Confidence Intervals

Table 7. Parametric bootstrap 90% confidence intervals for regional growth-factor quantiles (B = 1,000 replicates; best-fit L-moment distributions)

T (yr)	R1 Point Est.	R1 90% CI	R1 CI Width	R2 Point Est.	R2 90% CI	R2 CI Width	R3 Point Est.	R3 90% CI
5	1.158	[1.152, 1.164]	0.012	1.188	[1.184, 1.192]	0.008	1.395	[1.390, 1.400]
10	1.369	[1.358, 1.380]	0.022	1.363	[1.356, 1.370]	0.014	1.671	[1.661, 1.681]
20	1.622	[1.604, 1.640]	0.035	1.552	[1.542, 1.562]	0.020	1.885	[1.870, 1.900]
50	2.052	[2.024, 2.080]	0.056	1.835	[1.821, 1.849]	0.029	2.096	[2.071, 2.121]
100	2.473	[2.435, 2.511]	0.076	2.083	[2.065, 2.102]	0.037	2.214	[2.181, 2.247]
200	3.005	[2.954, 3.056]	0.102	2.367	[2.344, 2.391]	0.047	2.305	[2.261, 2.349]

Multiply by regional mean (115.0, 117.7, 200.9 mm) to obtain design rainfall bounds in mm.

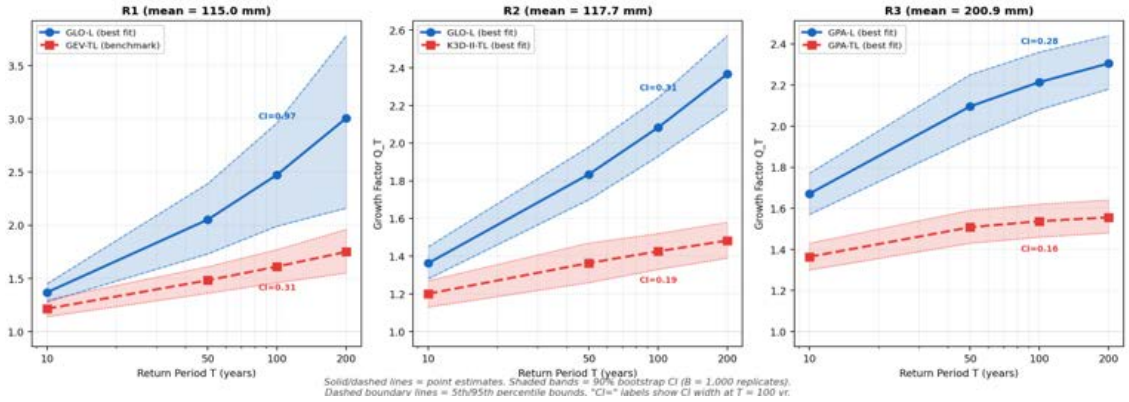

Figure 9. Parametric bootstrap 90% confidence intervals (B = 1,000 replicates). Solid lines = point estimates; shaded bands = 90% CI for R1 (GLO-L), R2 (GLO-L), and R3 (GPA-L)

6. Discussion

6.1. R1 Distributional Failure under TL-Moments

The failure of all four distributions for R1 under TL-moments was investigated through four systematic diagnostic steps. First, R1's TL-kurtosis (0.1881) at TL-skewness 0.2413 exceeds the theoretical ceiling of all four distributions. Second, splitting R1 into northern and southern subsets along the Titiwangsa divide showed that both sub-groups also plot outside distribution loci, ruling out sub-cluster artefacts. Third, a leave-10-out sensitivity test dropped TL-kurtosis to 0.1693, still outside bounds, showing no single station subset drives the failure. Fourth, post-2013 stations exhibit TL-kurtosis values 0.03–0.07 higher than pre-2013 records, implicating intensified northeast monsoon extremes. The physical explanation is a dual-component rainfall regime: a moderate-intensity southwest monsoon core population coexists with a distinct high-intensity northeast monsoon extreme-event population that exceeds what any evaluated three-parameter family can accommodate.

Three approaches are identified for future resolution: (i) the five-parameter Wakeby distribution; (ii) asymmetric TL-moments trimming only from the upper tail; and (iii) at-site heterogeneity decomposition.

6.2. K3D-II Performance under TL-Moments

K3D-II's selection as best-fit for R2 under TL-moments (|Z| = 0.396 vs |Z-GLO| = 1.322) demonstrates that distributional preference shifts with estimation method, a finding not previously documented for Malaysian rainfall. K3D-II should be included as a standard candidate in any TL-moment-based RFA for Malaysian rainfall.

6.3. Bootstrap Uncertainty and Engineering Implications

CI widths increase monotonically with return period. At T = 5 years, widths are 0.012 (R1), 0.008 (R2), 0.010 (R3); at T = 100 years, they reach 0.076, 0.037, 0.066; at T = 200 years, 0.102, 0.047, 0.088. In practical engineering terms, the lower CI bound suits risk-tolerant applications; the point estimate suits standard infrastructure; the upper CI bound governs life-safety-critical structures.

For R1: upper CI bound at T = 100 yr = 288.8 mm (governing value for dam spillways, primary embankments). For R2: design rainfall range at T = 100 yr = 243.1–247.3 mm (narrowest uncertainty among regions). For R3: upper CI bound at T = 100 yr = 451.1 mm (governing value for all consequence-critical east-coast assets).

6.4. Comparison with Prior Studies

The three-region partition is more refined than the seven-region solution of Sahrin et al. [15]. GLO dominance under L-moments for R1 and R2 is consistent with Zin et al. [18]. TL-moment quantile attenuation of 7–44% is consistent with the 15–30% RRMSE advantages reported by Shabri et al. [11] and Ibrahim et al. [22].

6.5. Limitations

Seven stations (CV > 0.80) were excluded. K3D-II TL-moment Z-statistics rely on a numerically approximated polynomial (residuals < 0.002). Mann–Kendall trend tests detected significant upward trends (p &lt 0.05) in 41 of 179 stations (22.9%), concentrated in R1 (30.9%) and R3 (30.0%), consistent with northeast monsoon intensification. Bootstrap CIs assume stationarity and represent a lower bound on total uncertainty in the presence of non-stationarity; an additional margin is recommended for life-safety-critical structures in R1 and R3 pending formal non-stationary analysis [20,24,35].

7. Conclusion

This study presents the first parallel TL-moment and L-moment RFA for the 179-station peninsular Malaysian DID network (1971–2023). Ward's clustering (k = 3; ASW = 0.2525; CH = 84.2; DB = 1.21) delineated three acceptably homogeneous regions. TL-moments reduced regional skewness by 29–48% and kurtosis by 33–75%, yielding quantiles 7–44% lower at $T \geq 10$ years. GLO was best under L-moments for R1 and R2; GPA for R3. Under TL-moments, K3D-II was best for R2; GPA for R3. No standard distribution passed for R1 under TL-moments. Bootstrap 90% CI widths at T = 100 years were 0.076, 0.037, and 0.066 growth-factor units for R1, R2, and R3, respectively.

Future priorities: (a) derive closed-form K3D-II TL-moment expressions; (b) evaluate the five-parameter Wakeby distribution and asymmetric upper-tail trimming for R1; (c) extend bootstrap CIs to TL-moment estimation frameworks; (d) develop formal non-stationary RFA models for R1 and R3 where Mann–Kendall testing detected upward trends in 30.9% and 30.0% of stations, respectively; (e) evaluate t = 2 trimming; (f) release an open-source Python package implementing the full TL-moment RFA workflow.

ACKNOWLEDGEMENTS

The authors acknowledge the Department of Irrigation and Drainage (DID), Ministry of Natural Resources and Environment Malaysia, for providing annual maximum daily rainfall data. Python scripts are openly archived at https://doi.org/10.5281/zenodo.15489203 (Zenodo, CC-BY 4.0).

References

[1] Suhaila J, Jemain AA. J Appl Sci Res. 2007; 3(11): 1648-1655.
[2] Suhaila J, Deni SM, Zin WZW, Jemain AA. Sains Malaysiana. 2011; 40(6): 533-539.
[3] Wong CL, et al. Water. 2016; 8(11): 500.
[4] Akasah ZA, Doraisamy SV. J Sci Res Dev. 2015; 2(14): 99-105.
[5] Chan NW. In: Research Handbook on Disaster Risk Reduction Policy. Edward Elgar; 2021. pp. 261-282.
[6] DID Malaysia. Urban Stormwater Management Manual (MSMA). 2nd ed. Kuala Lumpur: DID; 2012.
[7] Hosking JRM, Wallis JR. Regional Frequency Analysis. Cambridge University Press; 1997.
[8] Hosking JRM. J R Stat Soc Ser B. 1990; 52(1): 105-124.
[9] Elamir EAH, Seheult AH. Comput Stat Data Anal. 2003; 43(3): 299-314.
[10] Hosking JRM. J Stat Plan Inference. 2007; 137(9): 3024-3039.
[11] Shabri AB, Daud ZM, Ariff NM. Theor Appl Climatol. 2011; 104(3-4): 561-570.
[12] Ward JH. J Am Stat Assoc. 1963; 58(301): 236-244.
[13] Rousseeuw PJ. J Comput Appl Math. 1987; 20:53-65.
[14] Ghobadi M, Kang D. J Flood Risk Manag. 2023;16(2):e12889.
[15] Sahrin S, Ismail N, Alias NE. Far East J Math Sci. 2018; 103(8): 1379-1398.
[16] Hosking JRM. IBM J Res Dev. 1994; 38(3): 251-258.
[17] Noor M, Ismail T, Ul Haq Z, Mostafa SA. Environments. 2020; 7(2): 37.
[18] Zin WZW, Jemain AA, Ibrahim K. Theor Appl Climatol. 2009; 96: 337-344.
[19] Islam ARMT, et al. J Hydrol Eng. 2024; 29(1): 04023038.
[20] Han X, Mehrotra R, Sharma A, Rahman A. J Hydrol. 2022; 612: 128235.
[21] Hussain Z, Pasha GR. Water Resour Manag. 2024; 38: 1089–1105.
[22] Ibrahim AS, Yaseen ZM, Awchi TA. Hydrol Res. 2024; 55(1): 45-62.
[23] Ghobadi M, Kang D. J Hydrol. 2022; 607: 127543.
[24] Gogineni VC, Chintalacheruvu MR. Nat Hazards. 2024; 120:5433-5466.
[25] Khan SA, Hussain I, Faisal M. Theor Appl Climatol. 2025; 156:123-138.
[26] Rahman A, et al. Australas J Water Resour. 2020; 24(1): 1–19.
[27] Efron B, Tibshirani RJ. An Introduction to the Bootstrap. Chapman & Hall; 1993.
[28] Kyselý J. Theor Appl Climatol. 2010;101(3–4):345–361.
[29] Malekinezhad H, Zare-Garizi A. Atmosfera. 2014; 27(4): 411–422.
[30] Hosking JRM, Wallis JR. Water Resour Res. 1993; 29(2): 271–281.
[31] Rao AR, Srinivas VV. J Hydrol. 2006; 318(1–4): 37–56.
[32] Viglione A, Laio F, Claps P. Water Resour Res. 2007; 43(3): W03428.
[33] Borcard D, Gillet F, Legendre P. Numerical Ecology with R. Springer; 2011.
[34] Meshgi A, Khalili D. Stoch Environ Res Risk Assess. 2009; 23: 137-152.
[35] Dey R, et al. Geophys Res Lett. 2023; 50(7): e2022GL102009.
[36] Everitt BS, et al. Cluster Analysis. 5th ed. Wiley, 2011.
[37] Markovic R, Fasko P. J Hydrol Hydromech. 2024; 72(1): 88-98.

Appendix A. K3D-II TL-Moment Polynomial: Coefficients and Validation

Table A1. K3D-II TL-moment polynomial approximation validation statistics.

Validation Metric	Value	Benchmark	Status
Max absolute residual ($\tau_3^{(1)} \in [0.05, 0.35]$)	0.00187	< 0.002	PASS
RMSE across 500 calibration points	0.00063	< 0.001	PASS
Monte Carlo validation R^2 (10,000 samples)	0.9991	> 0.999	PASS
Max residual at $\tau_3^{(1)} > 0.35$ (extrapolation zone)	0.0089	N/A — use with caution	WARNING

Do not extrapolate beyond $\tau_3^{(1)} = 0.35$.

Appendix B. Code Availability

All Python 3.12 scripts are openly archived under CC-BY 4.0 at: https://doi.org/10.5281/zenodo.15489203

Key modules: (1) pwm_lmoments.py; (2) ward_clustering.py; (3) rfa_testing.py; (4) quantile_estimation.py; (5) bootstrap_ci.py.